Inorganic Chemistry

Article

pubs.acs.org/IC

Seven-Coordinate Lanthanide Sandwich-Type Complexes with a Tetrathiafulvalene-Fused Schiff Base Ligand

Feng Gao,[†] Long Cui,[†] Wei Liu,[‡] Liang Hu,[†] Yu-Wu Zhong,[§] Yi-Zhi Li,[†] and Jing-Lin Zuo*,[†]

[†]State Key Laboratory of Coordination Chemistry, School of Chemistry and Chemical Engineering, Nanjing National Laboratory of Microstructures, Nanjing University, Hankou Road 9, Nanjing 210093, People's Republic of China

[‡]College of Chemistry, Chemical Engineering and Materials Science, Soochow University, 199 Ren'ai Road, Suzhou 215006, People's Republic of China

[§]Beijing National Laboratory for Molecular Sciences, Institute of Chemistry, Chinese Academy of Sciences, North First Street 2, Beijing 100190, People's Republic of China

Supporting Information

ABSTRACT: Three seven-coordinate lanthanide(III) sandwich-type mononuclear complexes with π-conjugated TTF-Schiff base ligand H_2L (L^{2-} = 2,2′-((2-(4,5-bis(methylthio)-1,3-dithiol-2-ylidene)-1,3-benzodithiole-5,6-diyl)bis-(nitrilomethylidyne)bis(4-chlorophenolate)) and the tripodal ligand L_{OEt}^- (L_{OEt}^- = $[(\eta^5\text{-}C_5H_5)Co(P(=O)(OEt)_2)_3]^-$), $[(L_{OEt})Ln(L)]\cdot 0.25H_2O$ (Ln^{3+} = Dy^{3+}, **1**; Tb^{3+}, **2**; Ho^{3+}, **3**), have been synthesized and structurally characterized. All of the complexes are also characterized by absorption spectra and electrochemical, spectroelectrochemical, and magnetic studies. The Dy complex exhibits the field-induced slow relaxation of magnetization with an energy barrier of 41.6 K, indicating it shows single lanthanide-based SMM behavior. Introduction of the redox-active TTF unit into the sandwich-type lanthanide(III) complexes with interesting magnetic properties renders them promising for elaboration of new hybrid inorganic−organic materials.

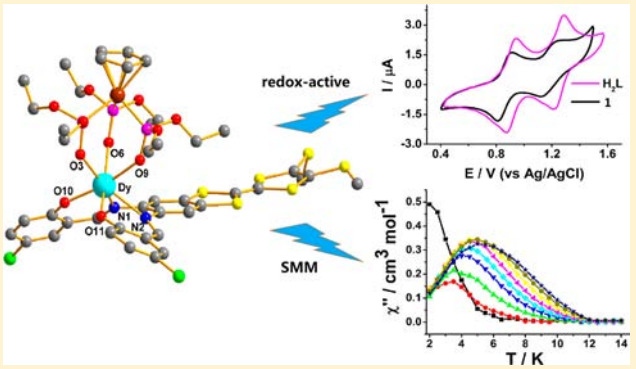

INTRODUCTION

Single-molecule magnets (SMMs) are molecular species that combine intramolecular properties of a high-spin ground state and large easy axis type magnetic anisotropy and exhibit out of phase contribution of the magnetic susceptibility. They are potentially useful in high-density data storage devices, quantum information processing, and molecular spintronics.[1] Thus far, many SMMs with various structures and magnetic properties have been reported.[2,3]

The need for new molecule-based materials that have more diversified properties is continuously increasing. One of the goals from scientists is to prepare materials that not only possess one expected property of function but also combine two or more of them in a multifunctional system. In particular, due to the important applications in molecular spintronics, the design and synthesis of new materials with both conductivity and magnetism has attracted more attention in recent years.[4] The objective of this combination is to establish a coupling between mobile and localized electrons, which mainly arise from organic moieties assembled in networks and paramagnetic metal ions. For preparation of conductive SMMs, one of representative strategies is to assemble redox-active tetrathiafulvalene (TTF) derivatives with the paramagnetic metal (3d transiton or 4f lanthanide) ions to construct new multifunctional materials with intriguing structures and interesting properties.[5,6] The reasons for the choice of the π-conjugated sulfur-rich compounds are as follows: (1) a conjugated sulfur-rich moiety that may show interchalcogen−atom interactions, which is often observed in molecule-based conductors; (2) investigation of the steric effects of the bulky ligand, which can have pronounced effects on the SMMs behavior; (3) attempts to construct conductive SMMs or molecular magnetic semiconductors. Moreover, comparing with the common 3d−π SMMs, it is particularly noteworthy that the 4f−π systems based on lanthanide ions may be good candidates for obtaining higher anisotropic barrier SMMs, which exhibit superparamagnet-like behavior of slow magnetic relaxation at low temperature.[7]

Recently, a series of mononuclear Ln−SMMs with the characteristic structures sandwiched by common Schiff base ligand, tetrapyrrole ligands (porphyrin or phthalocyanine), and the Kläui's tripodal ligand L_{OEt}^- (L_{OEt}^- = $[(\eta^5\text{-}C_5H_5)Co(P(=O)(OEt)_2)_3]^-$, Scheme 1, right) were reported by us.[8,9] In this paper, for the first time, the planar π-extended Schiff base ligand containing an electrochemically active TTF unit, 2,2′-((2-(4,5-

Received: June 5, 2013
Published: September 24, 2013

   dx.doi.org/10.1021/ic401421h | Inorg. Chem. 2013, 52, 11164−11172

Scheme 1. Structures of the TTF-Schiff Base Ligand H_2L and Kläui's Tripodal Ligand L_{OEt}^-

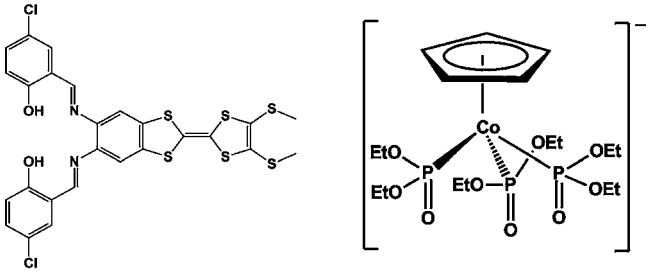

H_2L L_{OEt}^-

bis(methylthio)-1,3-dithiol-2-ylidene)-1,3-benzodithiole-5,6-diyl)bis(nitrilomethylidyne)bis(4-chlorophenol) (H_2L, Scheme 1, left), is introduced into this double-decker sandwich-type SMMs system. Three new lanthanide sandwich-type mononuclear complexes $[(L_{OEt})Ln(L)]\cdot 0.25H_2O$ (Ln^{3+} = Dy^{3+}, **1**; Tb^{3+}, **2**; Ho^{3+}, **3**) were obtained by reacting the TTF derivative and the tripodal ligand L_{OEt}^- with paramagnetic lanthanide ions. All of the complexes were structurally characterized, and their spectroscopic, electrochemical, and magnetic properties were studied. As is known, besides in SMMs, lanthanide sandwich-type multidecker complexes are also of interest in different areas such as molecular electronic sensors,[10] field-effect transistor devices,[11] etc. The synthetic method in this paper will extend further research on new multifunctional molecular materials, such as conductive sandwich-type SMMs.

EXPERIMENTAL SECTION

General Methods. All reagents were obtained from commercial sources and used without further purification. Starting materials $Na[(\eta^5\text{-}C_5H_5)Co\{P(=O)(OEt)_2\}_3]$ (NaL_{OEt}), 5,6-diamino-2-(4,5-bis(methylthio)-1,3-dithio-2-ylidene)benzo[*d*]-1,3-dithiole (diamino-TTF), and TTF-Schiff base ligand (H_2L) were synthesized according to the literature.[12−14] Elemental analyses for C, H, and N were carried out with a Perkin-Elmer 240C analyzer. ^{1}H NMR spectra were recorded on a Bruker DRX 500 spectrometer. Melting points were determined with an X-4 digital micromelting-point apparatus. Infrared spectra were recorded with a Vector22 Bruker spectrophotometer with KBr pellets in the range 400−4000 cm^{-1}. Cyclic voltammetry was performed with an Im6eX electrochemical analytical instrument using platinum as the working and counter electrodes, a Ag/AgCl electrode containing saturated KCl solution serving as the reference electrode, and 0.1 M n-Bu_4NClO_4 as the supporting electrolyte. UV−vis spectra were obtained with a UV-3600 spectrophotometer. Spectroelectrochemical measurements were performed by assembly of the electrochemical analytical instrument and UV−vis spectrophotometer. Magnetic susceptibility measurements were performed with a Quantum Design MPMS-SQUID-VSM magnetometer in the temperature range 1.8−300 K. The field dependence of magnetization was measured using a Quantum Design MPMS-SQUID-VSM system in an applied field of up to 70 kOe. Diamagnetic corrections were calculated using Pascal's constants,[15] and an experimental correction for the diamagnetic sample holder was applied.

X-ray Crystallography. Crystal structures were determined with a Siemens (Bruker) SMART CCD diffractometer using monochromated Mo Kα radiation (λ = 0.71073 Å) at 123 K. Cell parameters were retrieved using SMART software and refined using SAINT[16] for all observed reflections. Data was collected using a narrow-frame method with scan widths of 0.30° in ω and an exposure time of 10 s/frame. The highly redundant data sets were reduced using SAINT[16] and corrected for both Lorentz and polarization effects. Absorption corrections were applied using SADABS[17] supplied by Bruker. Structures were solved by direct methods using the program SHELXL-97.[18] Positions of metal atoms and their first coordination spheres were located from direct methods E-maps. Other non-hydrogen atoms were found in alternating difference Fourier syntheses and least-squares refinement cycles and, during the final cycles, refined

Table 1. Summary of Crystallographic Data for 1−3

	1·0.25H_2O	2·0.25H_2O	3·0.25H_2O
formula	$C_{43}H_{51}CoDyN_2O_{11}P_3S_6Cl_2\cdot 0.25H_2O$	$C_{43}H_{51}CoTbN_2O_{11}P_3S_6Cl_2\cdot 0.25H_2O$	$C_{43}H_{51}CoHoN_2O_{11}P_3S_6Cl_2\cdot 0.25H_2O$
fw	1353.96	1350.38	1356.39
cryst syst	monoclinic	monoclinic	monoclinic
space group	$P2_1/n$	$P2_1/n$	$P2_1/n$
a, Å	14.9211(15)	14.8268(17)	14.9021(19)
b, Å	19.9947(14)	19.9048(16)	20.1141(11)
c, Å	19.9744(14)	20.3778(17)	20.2924(15)
α, deg	90.00	90.00	90.00
β, deg	105.086(3)	105.300(3)	105.571(4)
γ, deg	90.00	90.00	90.00
V, Å^3	5753.8(8)	5800.8(9)	5859.3(9)
Z	4	4	4
ρ_{calcd}, g cm^{-3}	1.563	1.546	1.538
T/K	123(2)	123(2)	123(2)
μ, mm^{-1}	2.024	1.939	2.063
θ, deg	1.47−26.00	1.46−26.00	1.45−26.00
F(000)	2726	2722	2730
index ranges	$-10 \le h \le 18$	$-15 \le h \le 18$	$-17 \le h \le 18$
	$-24 \le k \le 22$	$-24 \le k \le 24$	$-18 \le k \le 24$
	$-24 \le l \le 24$	$-25 \le l \le 24$	$-25 \le l \le 22$
data/restraints/params	11 327/0/639	11 272/0/639	11 496/0/639
GOF (F^2)	1.068	1.072	1.036
R_1, $wR_2{}^a$ ($I > 2\sigma(I)$)	0.0607, 0.1489	0.0487, 0.1094	0.0524, 0.1351
R_1, $wR_2{}^a$ (all data)	0.0714, 0.1506	0.0591, 0.1112	0.0604, 0.1370

$^a R_1{}^a = \Sigma||F_o| - |F_c||/\Sigma|F_o|$. $wR_2 = [\Sigma w(F_o{}^2 - F_c{}^2)^2/\Sigma w(F_o{}^2)^2]^{1/2}$.

dx.doi.org/10.1021/ic401421h | Inorg. Chem. 2013, 52, 11164−11172

Scheme 2. Synthetic Route to the TTF-Schiff Base Ligand H_2L

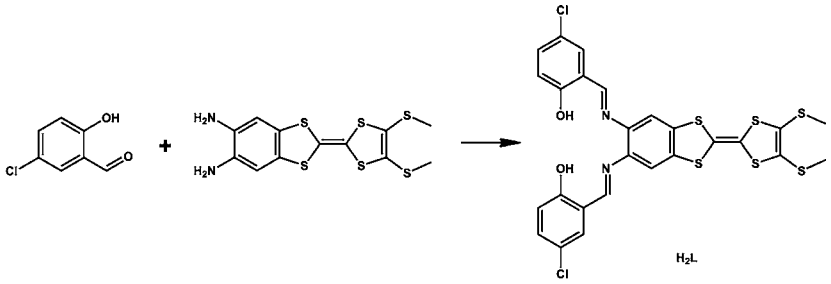

anisotropically. Hydrogen atoms were placed in calculated positions and refined as riding atoms with a uniform value of U_{iso}. Final crystallographic data and values of R_1 and wR_2 are listed in Table 1. CCDC reference numbers are 942329 (**1**), 942330 (**2**), and 942331 (**3**).

Computational Details. All calculations were carried out with Gaussian03 programs.[19] DFT and time-dependent DFT (TD-DFT) with the three-parameter B3LYP hybrid functional were employed.[20] Calculations were carried out using with a 6-31G* basis set for all atoms. All geometries were characterized as minima by frequency analysis (N_{imag} = 0).

Synthesis of TTF-Schiff Base Ligand (H_2L). 5,6-Diamino-2-(4,5-bis(methylthio)-1,3-dithio-2-ylidene)benzo[*d*]-1,3-dithiole (155 mg, 0.41 mmol) and 5-chloro-2-hydroxybenzaldehyde (128.9 mg, 0.82 mmol) were mixed in 50 mL of CH_2Cl_2/C_2H_5OH (1:4 v/v). The resulting mixture was stirred and heated at 70 °C for about 6 h, and the red precipitate was collected by filtration, washed with methanol, and then dried in air. Yield = 88%. Mp 275−277 °C. Anal. Calcd for $C_{26}H_{18}Cl_2N_2O_2S_6$: C, 47.77; H, 2.78; N, 4.29. Found: C, 48.11; H, 2.99; N, 4.57. ^{1}H NMR (500 MHz, C_5D_5N, 293 K): δ (ppm) 2.35 (s, 6H, SCH_3), 7.07 (d, 2H, J = 9.0 Hz, Ar-*H*), 7.31 (s, 2H, Ar-*H*), 7.37 (dd, 2H, J_1 = 9.0 Hz, J_2 = 1.5 Hz, Ar-*H*), 7.75 (d, 2H, J = 1.5 Hz, Ar-*H*), 8.83 (s, 2H, C*H*=N). IR (KBr, cm^{-1}): 3421(w), 2915(w), 1611(s), 1568(m), 1474(s), 1272(s), 1180(m), 1120(m), 922(s), 866(m), 774(m), 685(m). UV−vis {(CH_2Cl_2, λ_{max}/nm, [log (ε/dm^3 mol^{-1} cm^{-1})] in parentheses}: 269(4.62), 300(4.64), 332(4.62), 430(4.16).

Synthesis of [(L_{OEt})Dy(L)] (1). TTF-Schiff base Ligand (H_2L) (13.1 mg, 0.02 mmol), NaL_{OEt} (11.5 mg, 0.02 mmol), and $Dy(acac)_3 \cdot 2H_2O$ (9.2 mg, 0.02 mmol) were mixed in 10 mL of CH_3OH/MeCN (1:1 v/v). The reaction mixture was stirred and heated at 85 °C for 6 h and then filtered at room temperature. Orange block-shaped crystals of **1** were collected by filtration after slow evaporation of the resulting solution for several days. Yield = 45%. Mp > 300 °C. Anal. Calcd for $C_{43}H_{51}CoDyN_2O_{11}P_3S_6Cl_2$: C, 38.27; H, 3.81; N, 2.08. Found: C, 38.49; H, 4.02; N, 2.25. IR (KBr, cm^{-1}): 3414(w), 2972(w), 1608(s), 1516(m), 1457(m), 1374(m), 1241(w), 1130(s), 1031(m), 929(m), 830(m), 761(m), 584(m). UV−vis {(CH_2Cl_2, λ_{max}/nm, [log (ε/dm^3 mol^{-1} cm^{-1})] in parentheses}: 244(4.96), 300(4.68), 326(4.58), 414(4.53).

Synthesis of [(L_{OEt})Tb(L)] (2). Orange block-shaped crystals of **2** were obtained by following the same procedure as that described for **1** except that $Tb(acac)_3 \cdot 2H_2O$ was used in place of $Dy(acac)_3 \cdot 2H_2O$. Yield = 47%. Mp > 300 °C. Anal. Calcd for $C_{43}H_{51}CoTbN_2O_{11}P_3S_6Cl_2$: C, 38.37; H, 3.82; N, 2.08. Found: C, 38.55; H, 4.01; N, 2.23. IR (KBr, cm^{-1}): 3412(w), 2972(w), 1607(s), 1515(m), 1457(m), 1375(m), 1128(s), 1030(m), 928(m), 829(m), 760(m), 584(m). UV−vis {(CH_2Cl_2, λ_{max}/nm, [log (ε/dm^3 mol^{-1} cm^{-1})] in parentheses}: 243(4.98), 301(4.68), 326(4.61), 411(4.49).

Synthesis of [(L_{OEt})Ho(L)] (3). Orange block-shaped crystals of **3** were obtained by following the same procedure as that described for **1** except that $Ho(acac)_3 \cdot 2H_2O$ was used in place of $Dy(acac)_3 \cdot 2H_2O$. Yield = 45%. Mp > 300 °C. Anal. Calcd for $C_{43}H_{51}CoHoN_2O_{11}P_3S_6Cl_2$: C, 38.20; H, 3.80; N, 2.07. Found: C, 38.41; H, 4.05; N, 2.31. IR (KBr, cm^{-1}): 3410(w), 2972(w), 1609(s), 1514(m), 1458(m), 1377(m), 1130(s), 1030(m), 928(m), 830(m), 761(m), 584(m). UV−vis {(CH_2Cl_2, λ_{max}/nm, [log (ε/dm^3 mol^{-1} cm^{-1})] in parentheses}: 244(5.01), 300(4.73), 326(4.64), 416(4.60).

RESULTS AND DISCUSSION

Synthesis and Characterization. As indicated in Scheme 2, TTF-Schiff base ligand was synthesized by condensation reaction of 5-chlorosalicylaldehyde and the diamino-TTF derivative, which was developed by Liu et al.[14] Lanthanide complexes were successfully prepared by reaction of the TTF-Schiff base ligand, Kläui's ligand, and lanthanide acetylacetonates in methanol and acetonitrile. Introduction of the Cl atom into the ligand is to improve the solubility of the organic ligand, resulting in a straightforward synthesis of the complexes with moderate yield. All complexes are soluble in most organic solvents and air stable in both solution and the solid state. Characterization of these complexes has been accomplished by elemental analysis, IR, UV−vis, cyclic voltammetry, and single-crystal X-ray diffraction analysis.

Structural Description. Single-crystal X-ray diffraction analysis shows that all of the complexes crystallize in the monoclinic space group $P2_1/n$ with isostructual double-decker sandwich molecular structures. Selected bond lengths and angles are shown in Table 2. The Ln(III) ions (Ln^{3+} = Dy^{3+}, **1**; Tb^{3+}, **2**; Ho^{3+}, **3**) are seven coordinated and bonded with two nitrogen atoms from H_2L and five oxygen atoms (three from L_{OEt}^- and two from phenolic oxygen) (Figure 1a). An interesting 3:4 pseudo-piano-stool conformation can be used to describe the coordination geometry of the metallic core,[21] with the triangular plane formed by O3, O6, and O9 atoms from the L_{OEt}^- and the square base formed by O10, O11, N1, and N2 atoms from H_2L (Figure 1b). The Ln(III)−N bond length ranges from 2.498(5) to 2.512(6) Å, 2.489(4) to 2.520(4) Å, and 2.513(4) to 2.493(5) Å for **1**, **2**, and **3**, respectively, while the Ln(III)−O bond length is in the range 2.219(5)−2.296(4) Å for **1**, 2.219(4)−2.341(4) Å for **2**, and 2.212(5)−2.331(4) Å for **3**. Detailed structural parameters about average distances for Ln−N and Ln−O bond, Ln(III) to plane center distances (d_1, d_2), plane center distances (l), and bending angles of center−Ln(III)−center (α) for **1**−**3** are summarized in the Table 3. It is noted that the TTF core adopts a slightly boat-like conformation, and the dihedral angles between the two five-membered rings containing S atoms are 7.14(7)° for **1**, 7.02(4)° for **2**, and 6.78(5)° for **3**, whereas the intramolecular benzo-1,3-dithiole group is almost coplanar with a deviation of 2.39(8)°, 2.10(5)°, and 2.50(5)° for **1**, **2**, and **3**, respectively. In the crystal packing (Figure 2), the two neighboring TTF units are stacked head-to-tail with their molecular planes almost parallelly aligned, in which the centroid···centroid distance of the intermolecular benzene ring and 1,3-dithiole ring is 3.828(4) Å for **1**, 3.801(4) Å for **2**, and 3.806(5) Å for **3**. There is no obvious intermolecular

dx.doi.org/10.1021/ic401421h | Inorg. Chem. 2013, 52, 11164−11172

Table 2. Selected Bond Lengths (Angstroms) and Angles (degrees) for 1−3

	1	2	3
	bond distances (Å)		
Ln1−O3	2.266(5)	2.251(3)	2.242(4)
Ln1−O6	2.271(4)	2.256(3)	2.275(4)
Ln1−O9	2.296(4)	2.341(4)	2.331(4)
Ln1−O10	2.219(5)	2.263(3)	2.242(4)
Ln1−O11	2.233(5)	2.219(4)	2.212(5)
Ln1−N1	2.498(5)	2.489(4)	2.513(4)
Ln1−N2	2.512(6)	2.520(4)	2.493(5)
	bond angles (deg)		
O3−Ln1−O6	80.08(18)	80.41(13)	79.96(15)
O6−Ln1−O9	77.42(17)	77.57(12)	75.76(14)
O3−Ln1−O9	78.92(18)	79.81(13)	79.46(15)
O3−Ln1−O10	89.90(18)	89.51(13)	89.24(15)
O3−Ln1−O11	84.79(18)	84.50(14)	84.15(15)
O6−Ln1−O10	98.45(18)	98.47(13)	99.91(15)
O6−Ln1−O11	161.63(18)	161.54(12)	160.35(16)
O9−Ln1−O10	168.56(18)	169.07(13)	168.41(15)
O9−Ln1−O11	89.54(18)	89.39(13)	90.09(16)
O10−Ln1−O11	91.85(18)	91.93(13)	91.30(17)
O3−Ln1−N1	150.83(19)	150.49(14)	150.47(16)
O6−Ln1−N1	80.51(18)	80.39(12)	81.08(15)
O9−Ln1−N1	117.50(18)	117.32(12)	117.22(15)
O10−Ln1−N1	71.70(18)	71.46(12)	72.01(15)
O11−Ln1−N1	117.34(19)	117.55(13)	117.95(16)
O3−Ln1−N2	144.27(19)	143.85(14)	145.21(16)
O6−Ln1−N2	114.16(18)	113.78(13)	112.65(14)
O9−Ln1−N2	73.16(19)	71.86(13)	73.14(15)
O10−Ln1−N2	118.1(2)	118.88(13)	118.30(16)
O11−Ln1−N2	73.30(19)	73.42(13)	75.01(16)
N1−Ln1−N2	64.42(18)	65.23(13)	63.80(15)

shorter S···S contacts for them. The shortest intermolecular Ln^{3+}−Ln^{3+} distances are 10.845(8), 10.827(8), and 10.930(6) Å for **1**, **2**, and **3**, respectively.

Electrochemical Properties. Electrochemical properties of the compounds H_2L and **1**−**3** were investigated by cyclic voltammetry in CH_2Cl_2 as illustrated in Figure 3, and their electrochemical data are collected in Table 4. All compounds exhibit two well-separated reversible single-electron oxidation processes corresponding to successive oxidation of neutral TTF (TTF^0) to the radical cation ($TTF^{+\bullet}$) and then to the dication (TTF^{2+}). Moreover, the observed redox potentials of the oxidation processes for all of the complexes are slightly negatively shifted relative to H_2L. These potential shifts, although not very large, indicate that the electron-donating properties are changed due to the collaborative interaction of the deprotonation and coordination effects from the Schiff base (from phenol to phenolate) ligand, which are probably responsible for the small charge effects on the oxidation potential.[14,22]

Spectroscopic Properties. UV−vis absorption spectra for all of the reported compounds were measured in dichloromethane solution at room temperature (Figure 4). For the ligand H_2L, the electronic absorption spectrum displays intense transitions in the range 225−340 nm and a less intense broad absorption band around 430 nm, which mainly come from the spin-allowed $\pi-\pi^*$ transitions.[14,23] For complexes **1**−**3**, absorption spectra are quite similar to that of the free ligand H_2L. The absorption bands at low energy (λ > 350 nm) are slightly blue shifted, and the intensities are increased around 410−420 nm, which may be related to metalation of the ligand.[14]

To further investigate the redox process involving the TTF unit, spectroelectrochemical measurements were also carried out during electrolysis of the solution of H_2L and complexes **1**−**3** at suitable constant potentials (Figures 5 and S1, Supporting Information). The first stage of the electrochemical oxidation at the potential of about 1.0 V leads to formation of TTF radical cation with a broad absorption band emerging at about 830 nm for $H_2L^{+\bullet}$, 878 nm for $\mathbf{1}^{+\bullet}$, 881 nm for $\mathbf{2}^{+\bullet}$, and 879 nm for $\mathbf{3}^{+\bullet}$; meanwhile, the increase in the absorption intensity was observed around 440 nm for $H_2L^{+\bullet}$, 425 nm for $\mathbf{1}^{+\bullet}$, 427 nm for $\mathbf{2}^{+\bullet}$, and 424 nm for $\mathbf{3}^{+\bullet}$, respectively. Upon application of a potential of about 1.5 V, the electronic spectrum shows a decrease of the characteristic absorption of the radical cation bands and the broad absorption band around 830−880 nm is slightly blue shifted (around 718 nm for H_2L^{2+}, 732 nm for $\mathbf{1}^{2+}$, 735 nm for $\mathbf{2}^{2+}$, and 738 nm for $\mathbf{3}^{2+}$), which is the characteristic absorption band for the TTF dication. All

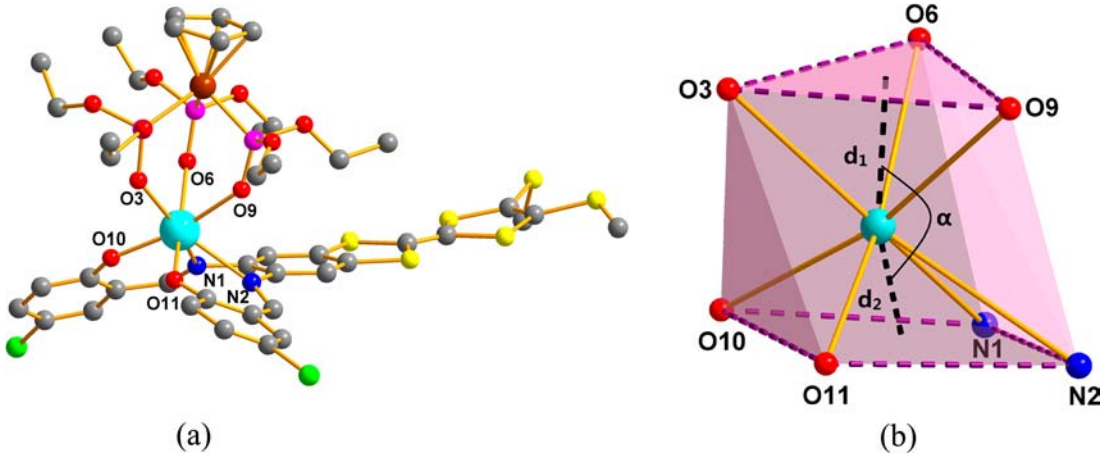

Figure 1. (a) Molecular structure of complexes [(L_{OEt})Ln(L)] (Ln = Dy, **1**; Tb, **2**; Ho, **3**). Solvates and H atoms are omitted for clarity: Ln, sky blue; Co, brown; O, red; N, blue; P, purple; S, yellow; C, gray; Cl, green. (b) Coordination geometry of Ln(III) core with d_1 and d_2 representing the distance of Ln(III) to the centers of the O3−O6−O9 plane and N1−N2−O10−O11 plane and the bending angle α, defined as the angle of center−Ln(III)−center.

dx.doi.org/10.1021/ic401421h | Inorg. Chem. 2013, 52, 11164−11172

Table 3. Summary of Average Distances for Ln−N and Ln−O Bond, Ln to Plane Center Distances, Plane Center Distances, Bending Angles, and Energy Barrier for 1, 2, 3, and Dy-salphen

	1−Dy	2−Tb	3−Ho	Dy−salphen
average Ln−N bond distance (Å)	2.505	2.509	2.503	2.478
average Ln−O bond distance (Å)	2.257	2.266	2.260	2.274
Ln to O3−O6−O9 plane center distance (d_1, Å)	1.549(4)	1.544(3)	1.561(3)	1.586(6)
Ln to N1−N2−O10−O11 plane center distance (d_2, Å)	1.222(3)	1.216(3)	1.214(3)	1.168(6)
center distance between O3−O6−O9 and N1−N2−O10−O11 planes (l, Å)	2.749(3)	2.737(3)	2.751(3)	2.717(5)
bending angle (α, deg)	165.30(15)	165.02(16)	164.91(15)	160.88(20)
$\Delta d^a = \lvert d_1 - d_2 \rvert$ (Å)	0.327	0.328	0.347	0.418
Δ/k_B [b] (K)	41.60			24.61

[a]Distance difference between the Ln(III) ion to centers of two planes. [b]Energy barrier based on the Arrhenius law [$\tau = \tau_0 \exp(\Delta/k_B T)$].

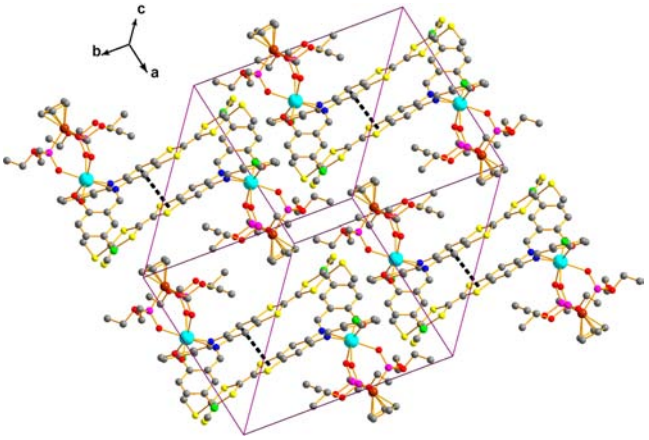

Figure 2. Crystal packing of complexes [(L_{OEt})Ln(L)] (Ln = Dy, **1**; Tb, **2**; Ho, **3**). Solvates and H atoms are also omitted for clarity: (dashed line) centroid···centroid distance of the intermolecular benzene ring and 1,3-dithiole ring.

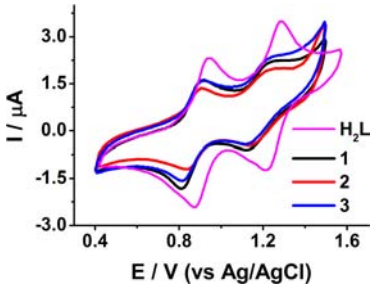

Figure 3. Cyclic voltammograms for compounds H_2L and **1**−**3** in CH_2Cl_2 (1.6×10^{-4} M) with n-Bu_4NClO_4 (0.1 M) at a sweep rate of 100 mV s^{-1}.

Table 4. Summary of Redox Potentials (V) for Compounds H_2L and 1−3

	E_{pc}^{ox1}	E_{pa}^{ox1}	$E_{1/2}^{ox1}$	E_{pc}^{ox2}	E_{pa}^{ox2}	$E_{1/2}^{ox2}$
H_2L	0.87	0.94	0.91	1.22	1.28	1.25
1	0.81	0.92	0.87	1.13	1.24	1.19
2	0.84	0.91	0.88	1.14	1.23	1.19
3	0.81	0.91	0.86	1.13	1.23	1.18

results suggest that the oxidation occurs at the TTF moiety in the present system.[24]

Computational Studies. DFT and TD-DFT calculations were performed to rationalize assignment of experimental absorption bands for H_2L and L_{OEt}^-. Calculated absorption spectra match well with the experimental ones.

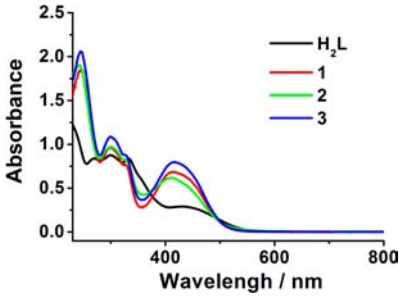

Figure 4. UV−vis absorption spectra for compounds H_2L and **1**−**3** in CH_2Cl_2 (2×10^{-5} M).

Molecular orbitals for H_2L involved in the main excited states are shown in Table 5 and Figures 6 and 7. The experimental absorption band around 430 nm corresponds to the predicted absorptions at 498, 460, and 427 nm, which mainly come from HOMO → LUMO, HOMO → LUMO+1, and HOMO → LUMO+2. These transitions dominantly possess $\pi_{TTF} \rightarrow \pi^*_{Schiff\ base}$ and $\pi_{TTF} \rightarrow \pi^*_{TTF}$ character. While the absorption peak at 332 nm can be attributed to combined transitions of $\pi_{TTF} \rightarrow \pi^*_{TTF}$, $\pi_{Schiff\ base} \rightarrow \pi^*_{Schiff\ base}$, and $\pi_{TTF\text{-}Schiff\ base} \rightarrow \pi^*_{Schiff\ base}$, and the peak center at 300 nm is of $\pi_{TTF\text{-}Schiff\ base} \rightarrow \pi^*_{Schiff\ base}$ and $\pi_{TTF\text{-}Schiff\ base} \rightarrow \pi^*_{TTF}$ character. In addition, the absorption at 269 nm mainly originates from $\pi_{Schiff\ base} \rightarrow \pi^*_{Schiff\ base}$ transitions, relevant to the calculated peak at 288 nm.

As shown in Table S1 and Figures S2 and S3 (Supporting Information), the absorption peak for L_{OEt}^- at 349 nm is assigned to $\pi_{cp} \rightarrow \pi^*_{cp}$ and MLCT transitions, which mainly involve HOMO, HOMO-1 to LUMO transitions at 404 nm. Calculations suggest the intense absorption at 250 nm is attributable to a combination of HOMO-2 → LUMO, HOMO-2 → LUMO+1, HOMO-3 → LUMO, and HOMO-4 → LUMO excitations, coming from combined $\pi_{cp} \rightarrow \pi^*_{cp}$ and $n_{O\ atoms} \rightarrow \pi^*_{cp}$ transitions.

Static Magnetic Properties. Temperature-dependent molar susceptibility data were measured for all of the complexes in the temperature range 1.8−300 K under an applied direct current (dc) field of 100 Oe. Room-temperature $\chi_M T$ values are 13.27 cm^3 K mol^{-1} for **1**, 11.74 cm^3 K mol^{-1} for **2**, and 13.79 cm^3 K mol^{-1} for **3**, which are slightly smaller than the theoretical values of 14.17 cm^3 K mol^{-1} for one uncoupled Dy(III) ($^6H_{15/2}$, $S = 5/2$, $L = 5$, $g = 4/3$, $J = 15/2$), 11.82 cm^3 K mol^{-1} for Tb(III) ($^7F_6$, $S = 3$, $L = 3$, $g = 3/2$, $J = 6$), and 14.07 cm^3 K mol^{-1} for Ho(III) ($^5I_8$, $S = 2$, $L = 6$, $g = 5/4$, $J = 8$) (Figure 8). On cooling, each $\chi_M T$ value gradually decreases, originating from depopulation of M_j states of the multiple

dx.doi.org/10.1021/ic401421h | Inorg. Chem. 2013, 52, 11164−11172

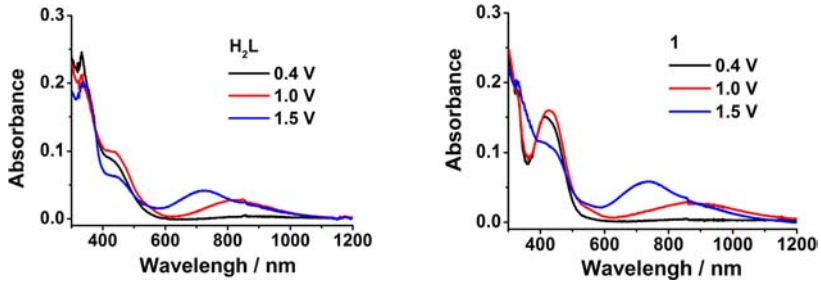

Figure 5. Spectroelectrochemistry for compounds H_2L and **1** in CH_2Cl_2/CH_3CN (1:1 v/v) (0.1 M n-Bu_4NClO_4).

Table 5. Main Calculated Optical Transitions for H_2L

orbital excitation	composition	main character	λ/nm (calcd)	f^a	λ/nm (exptl)
HOMO → LUMO	0.70432	$\pi_{TTF} \rightarrow \pi^*_{Schiff\ base}$	498	0.0845	430
HOMO → LUMO+1	0.67387	$\pi_{TTF} \rightarrow \pi^*_{Schiff\ base}$	460	0.1802	
HOMO → LUMO+2	0.19229	$\pi_{TTF} \rightarrow \pi^*_{TTF}$			
HOMO → LUMO+1	−0.18894	$\pi_{TTF} \rightarrow \pi^*_{Schiff\ base}$ and $\pi_{TTF} \rightarrow \pi^*_{TTF}$	427	0.0244	
HOMO → LUMO+2	0.67336				
HOMO → LUMO+2	0.68216	$\pi_{TTF} \rightarrow \pi^*_{TTF}$	378	0.2031	332
HOMO-7 → LUMO	−0.10353	$\pi_{Schiff\ base} \rightarrow \pi^*_{Schiff\ base}$ and $\pi_{TTF\text{-}Schiff\ base} \rightarrow \pi^*_{Schiff\ base}$	346	0.4658	
HOMO-2 → LUMO	−0.45011				
HOMO-1 → LUMO+1	0.48056				
HOMO-7 → LUMO	0.12630	$\pi_{Schiff\ base} \rightarrow \pi^*_{Schiff\ base}$	329	0.0750	
HOMO-2 → LUMO	0.64673				
HOMO-3 → LUMO	0.63406	$\pi_{TTF\text{-}Schiff\ base} \rightarrow \pi^*_{Schiff\ base}$	322	0.2925	
HOMO-6 → LUMO	0.30861	$\pi_{TTF\text{-}Schiff\ base} \rightarrow \pi^*_{Schiff\ base}$ and $\pi_{TTF\text{-}Schiff\ base} \rightarrow \pi^*_{TTF}$	296	0.3091	300
HOMO-1 → LUMO+2	0.30477				
HOMO-7 → LUMO	0.41134	$\pi_{Schiff\ base} \rightarrow \pi^*_{Schiff\ base}$	288	0.1242	269

[a]Oscillator strength.

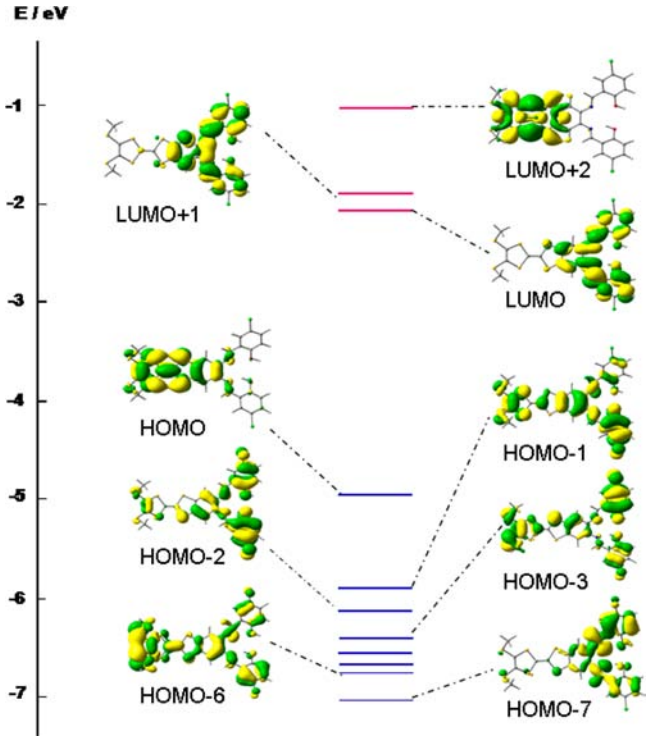

Figure 6. Molecular orbital energy diagram for H_2L. Pink bars represent unoccupied orbitals, and blue bars represent occupied orbitals.

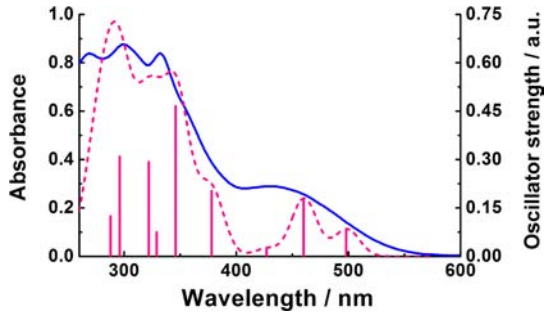

Figure 7. Experimental (blue line) and calculated (pink line) absorption spectra for H_2L.

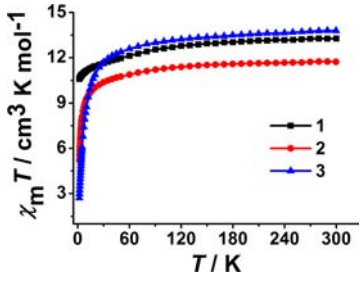

Figure 8. Temperature-dependent $\chi_M T$ values for **1**−**3** in the temperature range 1.8−300 K under an applied dc field of 100 Oe.

ground state[5c,7a,25,26] and/or possible weak antiferromagnetic interactions between molecules.[27]

M versus *H* plots for **1**−**3** from a zero dc field to 70 kOe at 1.8 K (Figure 9) show rapid increase in the magnetization at

dx.doi.org/10.1021/ic401421h | Inorg. Chem. 2013, 52, 11164−11172

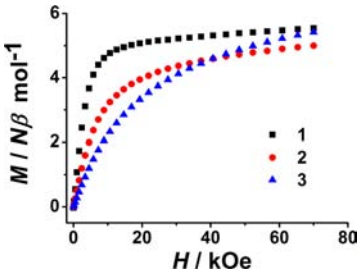

Figure 9. Field dependence of the magnetization data for **1**−**3** at 1.8 K.

low fields and then slowly reach a value of 5.54, 5.00, and 5.42 Nβ at 7 T for **1**, **2**, and **3**, respectively, which are lower than the expected saturation values of 10 Nβ for Dy and Ho and 9 Nβ for Tb, attributed to ligand-field-induced splitting of the M_j states of the multiple ground state.[7a,28]

Dynamic Magnetic Properties. To investigate the magnetization dynamics, alternative current (ac) magnetic susceptibility measurements were performed on all of the complexes in the temperature range 1.8−10.0 K at zero dc field. As the temperature is decreased, no out-of-phase (χ'') susceptibilities can be observed at a frequency of 999 Hz (Figures S4−S6, Supporting Information). By applying a dc field of 2 kOe, only the χ'' signals for **1** were enlarged above 1.8 K, showing a thermally activated dc-field-dependent relaxation phenomenon (Figure S7, Supporting Information). This behavior is attributed to suppression of quantum tunneling of magnetization (QTM) between sublevels, which is effective for Kramers' system with odd numbers of 4f electrons.[29] The Dy complex **1** belongs to this system, which has double-degenerate ground states at zero static field, and magnetization relaxation can occur through QTM mechanism. Upon application of a static field, the possibility of relaxation by this process disappears as the two states are not degenerate any longer, showing that the relaxation of such a two-level system may be governed by the second fastest path, such as Orbach or direct processes.[8,30] In contrast, for **2** and **3**, no similar χ'' signals under the same external dc field were observed above 1.8 K (Figures S8 and S9, Supporting Information). The reason is that Tb(III) and Ho(III) are non-Kramers' ions with a larger energy gap between the ground and the first excited states, along with their fast magnetization relaxation in SMMs.[29a]

For **1**, the temperature dependence of the in-phase (χ') and χ'' signals above a frequency of 666 Hz can be found under 2 kOe dc field. Unfortunately, the maximum peaks of χ'' in the temperature range 1.8−10.0 K were not obviously observed. In order to reduce the QTM effect, ac measurements were performed at 5.0 K with various applied dc field in the frequency range 1−999 Hz on complex **1** (Figure S10, Supporting Information). The results indicate that the QTM effect was minimized at 4 kOe static field, at which the ac susceptibilities become temperature and frequency dependent. This behavior characterizes a cross over from a direct phonon-induced tunneling process to an Orbach mechanism involving excited states.[31]

Under this optimum field, the peaks of χ'' signal can be observed at frequencies above 132 Hz in the temperature range 1.8−14.0 K (Figure 10a), and the relaxation process above 4.0 K follows a field-induced thermally activated mechanism. Fitting to the Arrhenius law [$\tau = \tau_0 \exp(\Delta/k_BT)$] afforded an energy barrier Δ/k_B = 41.60 K and the pre-exponential factor $\tau_0 = 9.2 \times 10^{-8}$ s (R = 0.9995) (Figure 10b), which is consistent with the expected τ_0 of 10^{-6}−10^{-11} s for similar SMMs.[32−34]

Variable-frequency ac magnetic susceptibility measurements were also carried out under 4 kOe dc field in the temperature range 4.0−6.0 K (Figure S11, Supporting Information). On cooling, the peaks of the χ'' signal show a slight shift from the high-frequency to the low-frequency region. The corresponding Cole−Cole plots show asymmetrically semicircular shapes and small tails in the high-frequency and low-frequency region, respectively (Figure S12, Supporting Information). Data in the high-frequency region can be fitted with a generalized Debye model,[35] affording α values of 0.20−0.31, which suggest the relaxation process followed a narrow width of the distribution above 4.0 K (Table S2, Supporting Information).

Recent studies indicate that slow relaxation of the magnetization in monometallic Ln−SMMs is closely related to 4f ion anisotropy and crystal field symmetry.[9,36] As summarized in Table 3, the following parameters d_1, d_2, l, and α can be used to effectively analyze the ligand-field effect on controlling the magnetic anisotropy of single-lanthanide SMMs. The energy barrier for **1** is higher than that of similar mononuclear

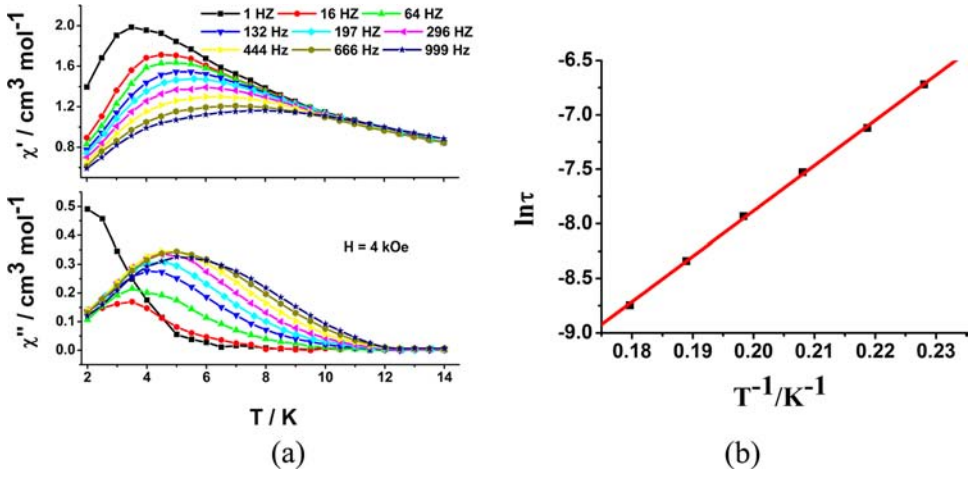

Figure 10. (a) Temperature-dependent in-phase (χ') and out-of-phase (χ'') ac susceptibilities for **1** under 4 kOe dc field. (b) Plots of ln τ vs T^{-1} for **1**. Red line represents the best fit to the Arrhenius law.

dx.doi.org/10.1021/ic401421h | Inorg. Chem. 2013, 52, 11164−11172

lanthanide complex based on common Schiff base ligand (**Dy-salphen**) as we previously reported,[8] suggesting the larger local symmetry and ligand-field effect in our present system. It may result from the improved planarity of the tetradendate Schiff base ligand after introduction of π-conjugated TTF unit. For **1**, the distances of Dy(III) to the O3−O6−O9 plane center and N1−N2−O10−O11 plane center are 1.549(4) and 1.222(3) Å, resulting in the difference Δd = 0.327 Å, whereas the related Δd for **Dy-salphen** is 0.418 Å. Additionally, the bending angles (α) for **1** (165.30(15)°) is higher than that of **Dy-salphen** (160.88(20)°). However, the energy barrier for **1** is still lower than that of classical eight-coordinate mononuclear lanthanide phthalocyaninato complexes.[3h] It is possibly attributed to the decreased coordination numbers and molecular symmetry, as well as the weakened strength of the ligand field for L_{OEt}^- compared to that of the phthalocyanine, that is, a slight structural difference may affect the nature of single-axial anisotropy of the Dy(III) ion through the single-axial ligand-field symmetry and therefore generate the different dynamic magnetic behavior.

CONCLUSION

Three new seven-coordinate paramagnetic lanthanide complexes with a planar π-conjugated Schiff base ligand containing an electrochemically active TTF unit and Kläui's tripodal ligand have been successfully synthesized. They exhibit the interesting double-decker sandwich coordination geometry, and spectroscopic and electrochemical studies suggest their reversible redox properties for classical TTF units. Only the Dy complex exhibits field-induced slow relaxation of magnetization, indicating that it shows single lanthanide-based SMM behavior. Introduction of a redox-active TTF unit into the sandwich-type lanthanide(III) complexes with interesting magnetic properties is helpful for further syntheses and studies on new hybrid inorganic−organic materials. More work to increase electric conductivity and enhance the d or f (metal)−π (radical) couplings as well as construct new molecular-based magnetic semiconductors is underway in our laboratory.

ASSOCIATED CONTENT

Supporting Information

Supplementary tables and figures and additional characterization data. This material is available free of charge via the Internet at http://pubs.acs.org.

AUTHOR INFORMATION

Corresponding Author

*Fax: +86-25-83314502. E-mail: zuojl@nju.edu.cn.

Notes

The authors declare no competing financial interest.

ACKNOWLEDGMENTS

This work was supported by the Major State Basic Research Development Program (2011CB808704 and 2013CB922101) and the National Natural Science Foundation of China (51173075 and 21021062). We also thank Prof. You Song and Dr. Tian-Wei Wang for experimental assistance on magnetic measurements.

REFERENCES

(1) (a) Christou, G.; Gatteschi, D.; Hendrickson, D. N.; Sessoli, R. *Mater. Res. Bull.* **2000**, *25*, 66. (b) Sessoli, R.; Gatteschi, D.; Caneschi, A.; Novak, M. A. *Nature* **1993**, *365*, 141. (c) Saitoh, E.; Miyajima, H.; Yamaoka, T.; Tatara, G. *Nature* **2004**, *432*, 203. (d) Bogani, L.; Wernsdorfer, W. *Nat. Mater.* **2008**, *7*, 179. (e) Leuenberger, M. N.; Loss, D. *Nature* **2001**, *410*, 789. (f) Yamanouchi, M.; Chiba, D.; Matsukura, F.; Ohno, H. *Nature* **2004**, *428*, 539. (g) Ward, M. D. *Coord. Chem. Rev.* **2007**, *251*, 1663. (h) Binnemans, K. *Coord. Chem. Rev.* **2009**, *109*, 4283.

(2) (a) Cornia, A.; Mannini, M.; Sainctavit, P.; Sessoli, R. *Chem. Soc. Rev.* **2011**, *40*, 3076. (b) Atanasov, M.; Comba, P.; Hausberg, S.; Martin, B. *Coord. Chem. Rev.* **2009**, *253*, 2306.

(3) (a) Murugesu, M.; Habib, F. *Chem. Soc. Rev.* **2013**, *42*, 3278. (b) Katoh, K.; Isshiki, H.; Komeda, T.; Yamashita, M. *Coord. Chem. Rev.* **2011**, *255*, 2124. (c) Sorace, L.; Benelli, C.; Gatteschi, D. *Chem. Soc. Rev.* **2011**, *40*, 3092. (d) Sessoli, R.; Powell, A. K. *Coord. Chem. Rev.* **2009**, *253*, 2328. (e) Zhang, P.; Guo, Y.-N.; Tang, J. *Coord. Chem. Rev.* **2013**, *257*, 1728. (f) Freedman, D. E.; Harman, W. H.; Harris, T. D.; Long, G. J.; Chang, C. J.; Long, J. R. *J. Am. Chem. Soc.* **2010**, *132*, 1224. (g) Ishikawa, N.; Mizuno, Y.; Takamatsu, S.; Ishikawa, T.; Koshihara, S. *Inorg. Chem.* **2008**, *47*, 10217. (h) Ishikawa, N.; Sugita, M.; Ishikawa, T.; Koshihara, S.; Kaizu, Y. *J. Am. Chem. Soc.* **2003**, *125*, 8694. (i) AlDamen, M. A.; Cardona-Serra, S.; Clemente-Juan, J. M.; Coronado, E.; Marti-Gastaldo, C.; Luis, F.; Montero, O. *Inorg. Chem.* **2009**, *48*, 3467. (j) AlDamen, M. A.; Clemente-Juan, J. M.; Coronado, E.; Marti-Gastaldo, C.; Gaita-Arino, A. *J. Am. Chem. Soc.* **2008**, *130*, 8874. (k) Liu, S.-J.; Zhao, J.-P.; Song, W.-C.; Han, S.-D.; Liu, Z.-Y.; Bu, X.-H. *Inorg. Chem.* **2013**, *52*, 2103.

(4) (a) Kosaka, Y.; Yamamoto, H. M.; Nakao, A.; Tamura, M.; Kato, R. *J. Am. Chem. Soc.* **2007**, *129*, 3054. (b) Coronado, E.; Day, P. *Chem. Rev.* **2004**, *104*, 5419. (c) Day, P.; Kurmoo, M. *J. Mater. Chem.* **1997**, *7*, 1291. (d) Motokawa, N.; Miyasaka, H.; Yamashita, M.; Dunbar, K. R. *Angew. Chem., Int. Ed.* **2008**, *47*, 7760. (e) Hiraga, H.; Miyasaka, H.; Nakata, K.; Kajiwara, T.; Takaishi, S.; Oshima, Y.; Nojiri, H.; Yamashita, M. *Inorg. Chem.* **2007**, *46*, 9661. (f) Kubo, K.; Shiga, T.; Yamamoto, T.; Tajima, A.; Moriwaki, T.; Ikemoto, Y.; Yamashita, M.; Sessini, E.; Mercuri, M. L.; Deplano, P.; Nakazawa, Y.; Kato, R. *Inorg. Chem.* **2011**, *50*, 9337.

(5) (a) Lorcy, D.; Bellec, N.; Fourmigué, M.; Avarvari, N. *Coord. Chem. Rev.* **2009**, 1398. (b) Enoki, T.; Miyazaki, A. *Chem. Rev.* **2004**, *104*, 5449. (c) Pointillart, F.; Le Guennic, B.; Maury, O.; Golhen, S.; Cador, O.; Ouahab, L. *Inorg. Chem.* **2013**, *52*, 1398. (d) Pointillart, F.; Le Guennic, B.; Golhen, S.; Cador, O.; Maury, O.; Ouahab, L. *Inorg. Chem.* **2013**, *52*, 1610. (e) Pointillart, F.; Golhen, S.; Cador, O.; Ouahab, L. *Dalton Trans.* **2013**, *42*, 1949. (f) Dupont, N.; Ran, Y.-F.; Liu, S.-X.; Grilj, J.; Vauthey, E.; Decurtins, S.; Hauser, A. *Inorg. Chem.* **2013**, *52*, 306. (g) Shao, M.-Y.; Huo, P.; Sun, Y.-G.; Li, X.-Y.; Zhu, Q.-Y.; Dai, J. *CrystEngComm* **2013**, *15*, 1086. (h) Pointillart, F.; Le Guennic, B.; Golhen, S.; Cador, O.; Maury, O.; Ouahab, L. *Chem. Commun.* **2013**, *49*, 615. (i) Pointillart, F.; Le Gal, Y.; Golhen, S.; Cador, O.; Ouahab, L. *Chem.—Eur. J.* **2011**, *17*, 10397.

(6) (a) Mitsumoto, K.; Nishikawa, H.; Newton, G. N.; Oshio, H. *Dalton Trans.* **2012**, *41*, 13601. (b) Cosquer, G.; Pointillart, F.; Le Guennic, B.; Le Gal, Y.; Golhen, S.; Cador, O.; Ouahab, L. *Inorg. Chem.* **2012**, *51*, 8488. (c) Branzea, D. G.; Fihey, A.; Cauchy, T.; El-Ghayoury, A.; Avarvari, N. *Inorg. Chem.* **2012**, *51*, 8545. (d) Xiong, J.; Li, G.-N.; Sun, L.; Li, Y.-Z.; Zuo, J.-L.; You, X,-Z. *Eur. J. Inorg. Chem.* **2011**, 5173. (e) Cosquer, G.; Pointillart, F.; Le Gal, Y.; Golhen, S.; Cador, O.; Ouahab, L. *Chem.—Eur. J.* **2011**, *17*, 12502. (f) Qin, Y.-R.; Zhu, Q.-Y.; Huo, L.-B.; Shi, Z.; Bian, G.-Q.; Dai, J. *Inorg. Chem.* **2010**, *49*, 7372. (g) Narayan, T. C.; Miyakai, T.; Seki, S.; Dinca, M. *J. Am. Chem. Soc.* **2012**, *134*, 12932. (h) Peng, Y.-H.; Meng, Y.-F.; Hu, L.; Li, Q.-X.; Li, Y.-Z.; Zuo, J.-L. *Inorg. Chem.* **2010**, *49*, 1905.

(7) (a) Rinehart, J. D.; Long, J. R. *Chem. Sci.* **2011**, *2*, 2078. (b) Katoh, K.; Horii, Y.; Yasuda, N.; Wernsdorfer, W.; Yoriumi, K.; Breedlove, B. K.; Yamashita, M. *Dalton Trans.* **2012**, *41*, 13582.

(8) Yao, M.-X.; Zheng, Q.; Gao, F.; Li, Y.-Z.; Song, Y.; Zuo, J.-L. *Dalton Trans.* **2012**, *41*, 13682.

(9) Gao, F.; Yao, M.-X.; Li, Y.-Y.; Li, Y.-Z.; Song, Y.; Zuo, J.-L. *Inorg. Chem.* **2013**, *52*, 6407.

(10) (a) Tada, H.; Touda, H.; Takada, M.; Matsushige, K. *Appl. Phys. Lett.* **2000**, *76*, 873. (b) Yasuda, T.; Fujita, K.; Tsutsui, T. *Chem. Phys. Lett.* **2005**, *402*, 395.
(11) (a) Chen, Y.; Su, W.; Bai, M.; Jiang, J.-Z.; Li, X.; Liu, Y.; Wang, L.; Wang, S. *J. Am. Chem. Soc.* **2005**, *127*, 15700. (b) Guillaud, G.; Al Sadoun, M.; Maitrot, M.; Simon, J.; Bouvet, M. *Chem. Phys. Lett.* **1990**, *167*, 503. (c) Jiang, J.-Z.; Ng, D. K. P. *Acc. Chem. Res.* **2009**, *42*, 79.
(12) Kläui, W.; Muller, A.; Eberspach, W.; Boese, R.; Goldbergs, I. *J. Am. Chem. Soc.* **1987**, *109*, 164.
(13) Guégano, X.; Kanibolotsky, A. L.; Blum, C.; Mertens, S. F. L.; Liu, S.-X.; Neels, A.; Hagemann, H.; Skabara, P. J.; Leutwvler, S.; Wandlowski, T.; Hauser, A.; Decurtins, S. *Chem.—Eur. J.* **2009**, *15*, 63.
(14) Wu, J.-C.; Liu, S.-X.; Keene, T. D.; Neels, A.; Mereacre, V.; Powell, A. K.; Decurtins, S. *Inorg. Chem.* **2008**, *47*, 3452.
(15) Boudreaux, E. A.; Mulay, L. N. *Theory and Application of Molecular Paramagnetism*; John Wiley & Sons: New York, 1976; p 491.
(16) *SAINT-Plus*, version 6.02; Bruker Analytical X-ray System: Madison, WI, 1999.
(17) Sheldrick, G. M. *SADABS an empirical absorption correction program*; Bruker Analytical X-ray Systems: Madison, WI, 1996.
(18) Sheldrick, G. M. *SHELXTL-97*; Universität of Göttingen: Göttingen, Germany, 1997.
(19) Frisch, M. J.; Trucks, G. W.; Schlegel, H. B.; Scuseria, G. E.; Robb, M. A.; Cheeseman, J. R.; Montgomery, Jr., J. A.; Vreven, T.; Kudin, K. N.; Burant, J. C.; Millam, J. M.; Iyengar, S. S.; Tomasi, J.; Barone, V.; Mennucci, B.; Cossi, M.; Scalmani, G.; Rega, N.; Petersson, G. A.; Nakatsuji, H.; Hada, M.; Ehara, M.; Toyota, K.; Fukuda, R.; Hasegawa, J.; Ishida, M.; Nakajima, T.; Honda, Y.; Kitao, O.; Nakai, H.; Klene, M.; Li, X.; Knox, J. E.; Hratchian, H. P.; Cross, J. B.; Bakken, V.; Adamo, C.; Jaramillo, J.; Gomperts, R.; Stratmann, R. E.; Yazyev, O.; Austin, A. J.; Cammi, R.; Pomelli, C.; Ochterski, J. W.; Ayala, P. Y.; Morokuma, K.; Voth, G. A.; Salvador, P.; Dannenberg, J. J.; Zakrzewski, V. G.; Dapprich, S.; Daniels, A. D.; Strain, M. C.; Farkas, O.; Malick, D. K.; Rabuck, A. D.; Raghavachari, K.; Foresman, J. B.; Ortiz, J. V.; Cui, Q.; Baboul, A. G.; Clifford, S.; Cioslowski, J.; Stefanov, B. B.; Liu, G.; Liashenko, A.; Piskorz, P.; Komaromi, I.; Martin, R. L.; Fox, D. J.; Keith, T.; Al-Laham, M. A.; Peng, C. Y.; Nanayakkara, A.; Challacombe, M.; Gill, P. M. W.; Johnson, B.; Chen, W.; Wong, M. W.; Gonzalez, C.; Pople, J. A. *Gaussian03, Revision B.04*; Gaussian, Inc.: Wallingford CT, 2004.
(20) (a) Lee, C.; Yang, W.; Parr, R. G. *Phys. Rev. B* **1988**, *37*, 785. (b) Miehlich, B.; Savin, A.; Stoll, H.; Preuss, H. *Chem. Phys. Lett.* **1989**, *157*, 200. (c) Becke, A. D. *J. Chem. Phys.* **1993**, *98*, 5648.
(21) (a) Girolami, G. S.; Milam, S. N.; Susllick, K. S. *Inorg. Chem.* **1987**, *26*, 343. (b) Kim, H.-J.; Whang, D.; Kim, K.; Do, Y. *Inorg. Chem.* **1993**, *32*, 360.
(22) (a) Wang, R.; Kang, L.-C.; Xiong, J.; Dou, X.-W.; Chen, X.-Y.; Zuo, J.-L.; You, X.-Z. *Dalton Trans.* **2011**, *40*, 919. (b) Li, G.-N.; Xiong, J.; Liao, Y.; Sun, L.; Li, Y.-Z.; Zuo, J.-L. *Polyhedron* **2011**, *30*, 2473. (c) Ran, Y.-F.; Steinmann, M.; Sigrist, M.; Liu, S.-X.; Hauser, J.; Decurtins, S. *C. R. Chim.* **2012**, *15*, 838. (d) Robson, K. C. K.; Koivisto, B. D.; Gordon, T. J.; Baumgartner, T.; Berlinguette, C. P. *Inorg. Chem.* **2010**, *49*, 5335.
(23) Khandar, A. A.; Shaabani, B.; Belaj, F.; Bakhtiari, A. *Inorg. Chim. Acta* **2007**, *360*, 3255.
(24) Perepichka, D. F.; Bryce, M. R.; Pearson, C.; Petty, M. C.; McInnes, E. J. L.; Zhao, J. P. *Angew. Chem., Int. Ed.* **2003**, *42*, 4636.
(25) Kahn, M. L.; Sutter, J. P.; Golhen, S.; Guionneau, P.; Ouahab, L.; Kahn, O.; Chasseau, D. *J. Am. Chem. Soc.* **2000**, *122*, 3413.
(26) Feng, W.-X.; Zhang, Y.; Zhang, Z.; Lü, X.-Q.; Liu, H.; Shi, G.-X.; Zou, D.; Song, J.-R.; Fan, D.-D.; Wong, W.-K.; Jones, R. A. *Inorg. Chem.* **2012**, *51*, 11377.
(27) Abbas, G.; Lan, Y. H.; Kostakis, G. E.; Wernsdorfer, W.; Anson, C. E.; Powell, A. K. *Inorg. Chem.* **2010**, *49*, 8067.
(28) Tang, J.-K.; Hewitt, I.; Madhu, N. T.; Chastanet, G.; Wernsdorfer, W.; Anson, C. E.; Benelli, C.; Sessoli, R.; Powell, A. K. *Angew. Chem., Int. Ed.* **2006**, *45*, 1729.
(29) (a) Sugita, M.; Ishikawa, N.; Ishikawa, T.; Koshihara, S.; Kaizu, Y. *Inorg. Chem.* **2006**, *45*, 1299. (b) Zhang, Y.-Z.; Duan, G.-P.; Sato, O.; Gao, S. *J. Mater. Chem.* **2006**, *16*, 2625.
(30) (a) Wang, H.-L.; Qian, K.; Wang, K.; Bian, Y.-Z.; Jiang, J.-Z.; Gao, S. *Chem. Commun.* **2011**, *47*, 9624. (b) Li, D.-P.; Wang, T.-W.; Li, C.-H.; Liu, D.-S.; Li, Y.-Z.; You, X.-Z. *Chem. Commun.* **2010**, *46*, 2929. (c) Jiang, S.-D.; Wang, B.-W.; Su, G.; Wang, Z.-M.; Gao, S. *Angew. Chem., Int. Ed.* **2010**, *49*, 7448. (d) Vallejo, J.; Castro, I.; Garcia, R. R.; Cano, J.; Julve, M.; Lioret, F.; Munno, G. D.; Wernsdorfer, W.; Pardo, E. *J. Am. Chem. Soc.* **2011**, *134*, 15704. (f) Ishikawa, N.; Sugita, M.; Wernsdorfer, W. *J. Am. Chem. Soc.* **2005**, *127*, 3650. (g) Langley, S. K.; Chilton, N. F.; Ungur, L.; Moubaraki, B.; Chibotaru, L. F.; Murray, K. S. *Inorg. Chem.* **2012**, *51*, 11873.
(31) (a) Ishikawa, N.; Sugita, M.; Ishikawa, T.; Koshihara, S.-Y.; Kaizu, Y. J. *Phys. Chem. B* **2004**, *108*, 11265. (b) Ren, M.; Bao, S.-S.; Hoshino, N.; Akutagawa, T.; Wang, B.; Ding, Y.-C.; Wei, S.; Zheng, L.-M. *Chem.—Eur. J.* **2013**, *19*, 9619.
(32) Cole, K. S.; Cole, R. H. *J. Chem. Phys.* **1941**, *9*, 341.
(33) Ishii, N.; Okamura, Y.; Chiba, S.; Nogami, T.; Ishida, T. *J. Am. Chem. Soc.* **2008**, *130*, 24.
(34) Aubin, S. M.; Sun, Z.; Pardi, L.; Krzystek, J.; Folting, K.; Brunel, L. C.; Rheingold, A. L.; Christou, G.; Hendrickson, D. N. *Inorg. Chem.* **1999**, *38*, 5329.
(35) Katoh, K.; Kajiwara, T.; Nakano, M.; Nakazawa, Y.; Wernsdorfer, W.; Ishikawa, N.; Breedlove, B. K.; Yamashita, M. *Chem.—Eur. J.* **2011**, *17*, 117.
(36) Gonidec, M.; Luis, F.; Vílchez, À.; Esquena, J.; Amabilino, D. B.; Veciana, J. *Angew. Chem., Int. Ed.* **2010**, *49*, 1623.